Supplementary Information

Rapid kinetic fingerprinting of single nucleic acid molecules by a FRET-based dynamic nanosensor

Kunal Khanna[1,†], Shankar Mandal[1,†], Aaron T. Blanchard[1,2,3], Muneesh Tewari[2,4,5,6], Alexander Johnson-Buck[1,4,5,], and Nils G. Walter[1,5,6,*]*

[1]Single Molecule Analysis Group, Department of Chemistry, University of Michigan, Ann Arbor, Michigan, 48109, United States
[2]Department of Biomedical Engineering, University of Michigan, Ann Arbor, Michigan, 48109, United States
[3]Michigan Society of Fellows, University of Michigan, Ann Arbor, Michigan 48109, United States
[4]Department of Internal Medicine, Division of Hematology/Oncology, University of Michigan, Ann Arbor, Michigan, 48109, United States
[5]Center for RNA Biomedicine, University of Michigan, Ann Arbor, Michigan, 48109, United States
[6]Center for Computational Medicine and Bioinformatics, University of Michigan, Ann Arbor, Michigan, 48109, United States

* To whom correspondence should be addressed. Tel: +1 734 615 2060; Email: nwalter@umich.edu
Correspondence may also be addressed: Email: alebuck@umich.edu

† These authors contributed equally to this work

Present Address: Alexander Johnson-Buck, aLight Sciences, Inc., 333 Jackson Plz Suite 460, Ann Arbor, Michigan, 48103, United States

Table of contents

1. Supplementary texts

1.1 Preparation of slides, coverslips, and sample cells

Single-molecule fluorescence microscopy experiments were performed using either an objective-TIRF or a prism-TIRF microscope, which required different protocols for preparing slides or coverslips and sample cells as previously described (Abelson et al., 2010; Johnson-Buck et al., 2019). Objective-TIRF coverslips and imaging cells were prepared by following three basic steps: cleaning the coverslip to remove organic residues from surface, passivating the surface with affinity tags, and preparing the sample cells by attaching cut pipette tips as described previously (Chatterjee et al., 2020; Hayward et al., 2018). Briefly, VWR No. 1.5, 24×50 mm coverslips (VWR, catalog no. 48393-241) were cleaned following either one of two procedures. In one cleaning procedure, the coverslips were cleaned by applying plasma for 3 min and then washed two times with acetone. In the second cleaning procedure, the coverslips were first sonicated for 10 min in acetone, then sonicated in 1M KOH for 20 min, and finally were treated with "base piranha" solution consisting of 14.3% v/v of 28-30 wt% NH_4OH, and 14.3% v/v of 30-35 wt% H_2O_2 that was heated to 70-80°C before immersing the slide in it as previously described (Chatterjee et al., 2020). Following either cleaning procedure, coverslips were then modified to present surface amines by mounting them in a coplin jar and submerging them in a 2% v/v solution of (3-aminopropyl) triethoxysilane (APTES) (Sigma-Aldrich, catalog no. A3648-100ML) in acetone for 10 min, sonicating the jar for 1 min, incubating for another 10 min, rinsed twice with acetone, rinsed five times with water, and dried with nitrogen. Slides were then functionalized by sandwiching a 1:10 or 1:100 mixture of biotin-PEG-succinimidyl valerate and methoxy-PEG-succinimidyl valerate (Laysan Bio, Inc. catalog no. BIO-PEG-SVA-5K-100MG & MPEG-SVA-5K-1g) in 0.1M $NaHCO_3$ with a final mPEG concentration of 0.25 mg/μL and a final biotin PEG concentration of 0.0025 or 0.025 mg/μL for 1:100 or 1:10 mixtures, respectively, between pairs of coverslips. To reduce nonspecific binding of nucleic acids to the surface, the remaining surface amines were quenched by sandwiching ~80 μL of 0.03 mg/μL disulfosuccinimidyltartrate (Soltec Ventures, catalog no. CL107) in 1M $NaHCO_3$ between pairs of coverslips. Finally, the coverslips were dried completely under nitrogen flow and stored in the dark under air for further use for up to 3 weeks. The sample cells were prepared prior to the single-molecule experiments using 20 μL pipet tips (ART low retention, Thermo Scientific). Specifically, a razor blade was used to cut through the diameter of a pipette tip ~2 cm from the wide end of the pipette tip and the noncut base was attached to the functionalized coverslip via epoxy (Ellsworth adhesives, hardman double, catalog no. 4001) (Hayward et al., 2018). Four pipette tips were generally attached to each coverslip in this manner. The 1:10 PEG ratio coverslips were used for objective-TIRF miR-141 optimization experiments and the 1:100 PEG ratio was used for all optimization and quantification experiments for *EGFR* exon 19 deletion mutant DNA (*EGFR*Δ_{exon_19}) and quantification experiments only for miR-141RNA. Additionally, all objective-TIRF miR-141 quantification experiments used plasma cleaning while all *EGFR*Δ_{exon_19} experiments used piranha cleaning and miR-141 optimization used mostly piranha with some plasma cleaning. Both cleaning protocols showed very similar analytical performance (Fig. S15). For prism TIRF experiments, the fluidic sample cells were

constructed using two pieces of double-sided tape sandwiched between a microscope slide and glass coverslip (VWR 22×30 mm). Each microscope slide had a hole on each of two ends, which was connected to Tygon tubing for exchanging sample solutions and buffers. Prior to assembly of the sample cell, the microscope slide's surface was cleaned using an aqueous solution of "base piranha" as described above. The microscope slides were often reused by heating the slides in warm to boiling water to loosen the glue and remove the coverslip, followed by removal of all remaining residue with a razor blade and subsequent Alconox paste and base piranha cleaning.

1.2 Prism-type TIRF iSiMREPS assay for detection of miR-141

To detect miR-141 using a prism-TIRF microscope (Fig. 2), a fluidic sample cell was first passivated by injecting 150 µL of 1 mg/mL biotin-BSA (Thermo Fischer, 25mg ImmunoPure) for 10 min to coat the slide surface with biotin-BSA. The chamber was then washed out with T50 (10 mM Tris pH 8.0 at 25°C, 50 mM NaCl) and 150 µL of streptavidin at 1mg/mL concentration was flowed into the chamber, and the streptavidin was allowed to incubate for 10 min to bind with the biotin-BSA. The unbound streptavidin was then washed out with 4× PBS (Phosphate-buffered saline, pH 7.4 at 25°C). Next, 150 µL of preassembled iSiMREPS sensors bound with miR-141 were injected into the chamber for tethering onto the slide surface via biotin-streptavidin linkages. The sensors used for this step were assembled by combining the anchor, capture, and query probes as well as the miR-141 target at 1.000:1.125:1.125:1.250 ratios respectively at approximately 100 pM final concentration in 150 µL solutions in 4× PBS buffer. After combining, the sensors were heated at 70˚C for 7 min in a metal bath and then cooled at room temperature for 20 min. To prolong the lifetimes of fluorophores and thus obtain more accurate measurements of the FRET signals, an imaging buffer containing an oxygen scavenger system (OSS) consisting of 1 mM Trolox, 5 mM 3,4-dihydroxybenzoate, and 50 nM protocatechuate dioxygenase in 4× PBS was injected into the chamber prior to imaging under a prism-TIRF microscope.

1.3 Exponential fitting of the cumulative frequency of dwell times

Average dwell times for a given experiment were processed using a custom MATLAB (version 2019a or later) script. The script first determined the cumulative frequency of all the dwell times for a given state using bins the size of the camera exposure time (0.06-0.1 s). This cumulative frequency was then fit to either a single exponential function (*Equation S1*) or a double exponential function (*Equation S2*):

$$y = ae^{-x/\tau} + c \qquad (S1)$$

$$y = ae^{-x/\tau 1} + be^{-x/\tau 2} + c \qquad (S2)$$

where a, b, c, τ, $\tau 1$ and $\tau 2$ are fit parameters. The coefficients a and b are used to fit the function and for the double exponential, determine the weight of each term for plotting, and obtaining average dwell times. The coefficient τ describes, for the single exponential fit, the average dwell time for a given event. The coefficients $\tau 1$ and $\tau 2$ describe, for the double exponential fit, the average dwell time for shorter- and

longer-lived populations of events, respectively. The coefficient c is a constant the gives the y-intercept for the equation.

For each dataset, the cumulative frequency was first fit to the single exponential fitting function. This fit was then kept if the sum squared error < 0.05 and the R^2 > 0.98 for detecting miR-141 and the sum squared error < 0.08 and the R^2 > 0.96 for detecting *EGFR* exon 19 deletion mutant DNA (*EGFR*Δ_{exon_19}), which indicated a good fit and suggested that the coefficient t was an accurate average dwell time. If these conditions were not met, a double exponential function (equation S2) was used instead, and the average dwell time was calculated as $\tau = (a\tau 1 + b\tau 2)/(a + b)$. This equation calculated a weighted average of both populations that was reported as the average dwell time for the entire data set.

1.4 Statistical mechanical simulations of iSiMREPS sensors

Simulations were performed using a Monte Carlo simulation method described by Becker, Rosa, and Everaers (Becker et al., 2010). In this method, each ssDNA nucleotide (nt) or dsDNA base pair (bp) was represented as a point at fixed distance from its neighbors, h (0.6 nm/nt for ssDNA (Saleh et al., 2009) or 0.34 nm/bp for dsDNA (Marko and Siggia, 1995)), and then a series of 10^7 iterations were applied to the construct via the Metropolis-Hastings algorithm. Each iteration consisted of a pivot attempt, which entails selection of a random point in the construct, followed by a counterclockwise rotation of all downstream points (where upstream means closer to the point at which the construct is anchored to the surface) around a random axis by an angle randomly sampled from the range $\pm 50°$. The construct's post-pivot free energy, G, was calculated as the sum of the bending energy of all non-terminal points. The bending energy for the i^{th} non-terminal point (e.g., a point that is bound to at least two additional points), g_i, with 3D coordinate vector $\boldsymbol{r_i}$ is:

$$g_i = -k_{s,i}\frac{(\boldsymbol{r}_i - \boldsymbol{r}_{i\leftarrow}) \cdot (\boldsymbol{r_i} - \boldsymbol{r}_{i\rightarrow})}{|\boldsymbol{r_i} - \boldsymbol{r}_{i\leftarrow}||\boldsymbol{r_i} - \boldsymbol{r}_{i\rightarrow}|} \qquad (S3)$$

where $k_{s,i}$ is the point's bending spring constant, which is related to the persistence length, L_p (1.4 nm for ssDNA(Chen et al., 2012) or 53 nm for dsDNA(Marko and Siggia, 1995), via the relation

$$L_p = \frac{-h}{\ln\left(coth(k_s) - \frac{1}{k_s}\right)} \qquad (S4)$$

and $r_{i\leftarrow}$ and $r_{i\rightarrow}$ are the 3D coordinate vectors for the nearest upstream and downstream points, respectively. (Note that for single-stranded RNA in the miR-141 design, we used $L_p = 0.8\,nm$ and $h = 0.67\,nm$) (Seol et al., 2004). Next, G was calculated as $G = \sum g_i$ and the change in G from the last iteration, ΔG, was used to determine whether the pivot is accepted. Specifically, the pivot was accepted if $\Delta G < 0$ or, in the scenario that $\Delta G > 0$, if $\exp(-\Delta G) > R$, where R is a randomly generated number sampled from the range of 0 to 1. To reflect attachment of the construct to a surface, G was set to ∞ if any point in the construct exhibited a z-position below 0. Regardless of whether or not the pivot was accepted, the inter-strand distance was calculated at the end of each iteration as the average of the

distances between the pairs of nucleotides that pair together to form the query-target duplex or the competitor-query duplex.

1.5 Optimization of iSiMREPS sensor concentration, invaders, and target incubation time to increase the sensitivity of detecting *EGFR* exon 19 deletion mutant DNA (*EGFR*Δ_{exon_19}).

The iSiMREPS sensor is used to count surface-immobilized analyte molecules via a TIRF microscopy setup. Thus, the sensitivity of iSiMREPS is limited by the diffusion of target molecules to the surface, as well as the kinetics and thermodynamics of binding between the target and capture probe. The number of surface-immobilized target molecules can be enhanced by increasing the density of sensors on the surface as well incubating target solution for a longer duration. However, higher sensor density results in higher background signal, which can be addressed with higher invader concentration and/or longer invader incubation time. To increase the sensitivity of iSiMREPS, we therefore tested the performance of the sensor $Q_8C_6QS_{18}CS_{19}$ with different probe concentrations, invaders, and target incubation times.

First, the performance of the sensor was tested using 10, 25, and 50 nM sensor to detect 10 pM *EGFR* exon 19 deletion mutant DNA (*EGFR*Δ_{exon_19}). The target was incubated for 90 min and pretreated with 2.5 μM invaders for 20 min to remove non-target bound sensors before imaging. The results showed that S/N values in the target bound traces decreased as sensor concentration increased (Fig. S12A). However, the number of accepted traces per FOV was highest when 25 nM sensor was used (Fig. S12A). This can potentially be explained as follows: with 10 nM sensor, the surface density of sensor was insufficient to efficiently capture target molecules, resulting in low counts; with 50 nM sensor, the imaging surface was saturated with target bound molecules, resulting in high background. Since 25 nM probe showed good S/N and more accepted traces per FOV, we considered this concentration for further optimization of assay conditions.

Next, we varied the incubation time of invaders (5, 10, 20, 25, and 30 min) while holding all other parameters and assay conditions equal. The number of accepted counts increased roughly linearly with the invader's incubation time and flatlined at 20 min. Therefore, 20 min was chosen as the optimized invader incubation time (Fig. S12B). Finally, we tested the effect of target incubation time on the sensitivity of the sensor. We varied the target incubation time (30, 60, 90 and 120 min) while holding all other parameters and assay conditions equal. The results showed that the number of accepted traces increased with the target incubation time, peaked 90 min, declined at 120 min (Fig. S12C). It is possible that at 120 min, some sensors dissociated from the surface. Therefore, a target incubation time of 90 min was chosen for further experimentation.

1.6 Calculation of specificity for detection of *EGFR* exon 19 deletion mutant DNA (*EGFR*Δ_{exon_19}).

The specificity of the iSiMREPS assay for detecting *EGFR* exon 19 deletion mutant (MUT) DNA in the presence of wild-type (WT) DNA was calculated based on a previously-published protocol(Hayward et al., 2018). Briefly, to determine specificity, 500 fM MUT DNA was spiked into 50 or 500 nM WT DNA to obtain a mutant allelic fraction of 0.001 or 0.0001%, respectively. These samples were analyzed using an objective-type TIRF microscope as described in the Methods section in the main text. MUT-free samples with 50 or 500 nM WT were used as controls. The specificity was then calculated from the number of true negative (*TN*) and false positive (*FP*) counts using the following relationship.

$$Specificity = \frac{TN}{TN+FP} \quad (S5)$$

TN is equal to the number of WT molecules within the field of view that are not detected as MUT and *FP* is equal to the number of false positives in a WT-only experiment.

$$TN = (Number\ of\ WT\ molecules\ in\ FOV) - FP \quad (S6)$$

In an iSiMREPS assay, the number of WT molecules per field of view can be estimated by assuming that the kinetics of capture are identical for MUT and WT molecules with the equation below.

$$Number\ of\ WT\ molecules\ in\ FOV = TP \times (C_{WT} / C_{MUT}) \quad (S7)$$

C_{WT} and C_{MUT} are the concentrations of WT and MUT molecules, respectively, and *TP* is the number of true positives within the field of view.

$$Number\ of\ true\ positives\ (TP)\ in\ FOV = (Number\ of\ counts\ in\ MUT + WT) - (Number\ of\ counts\ in\ WT\text{-}only) \quad (S8)$$

$$TN = TP \times (C_{WT}/C_{MUT}) - FP \quad (S9)$$

By substituting equation (S9) into equation (S5), we obtain

$$Specificity = 1 - \frac{FP}{TP \times (C_{WT}/C_{MUT})} \quad (S10)$$

1.7 Processing and analysis of prism-TIRF data

The prism-TIRF movies were processed with MATLAB scripts that detected areas of higher intensity that correspond to potential molecules and used a bead mapping procedure (Abelson et al., 2010) to pair donor and acceptor signals in both channels coming from the same molecules. These scripts generated trace files that were analyzed with other scripts, where traces that showed transitions between FRET states (indicative of fingerprint generation) were selected for further analysis of their kinetics and FRET distribution. The criteria for which traces were accepted or rejected is outlined in Table S5. The traces, once selected, were then further processed with MATLAB scripts to obtain FRET values and time data that could be inputted into QuB (University of Buffalo software). QuB was then used to create an idealized hidden Markov model (HMM) (Bronson et al., 2009) to assign FRET states for all traces at each time. Idealized trace data from QuB was then further processed with MATLAB scripts to do two things: (1) Obtain dwell times in the low and high-FRET states and an average dwell time per state through cumulative frequency exponential fitting (see SI above, and Fig. S2), and (2) Obtain transition occupancy density plots (TODPs) which show the frequency of molecules exhibiting transitions between

particular pairs of FRET states (Blanco and Walter, 2010). These average dwell times and TODPs were used to evaluate the sensor performance.

2. Supporting Tables

Table S1. The list of oligonucleotides used for detection of miR-141.

ID	Sequence: 5´-3´	Usage
miR-141	UAACACUGUCUGGUAAAGAUGG	All sensors
Capture_miR-141	/5Cy3/C+A+GAC+A+GTGTTATTTGGCGGAGTGTCC	All sensors
Query_Q_8QS_3	CGCGGCCCAGGATTTCCATCTTT/3AlexF647N/	All sensors with Q_8QS_3
Query_Q_8QS_{18}	CGCGGCCCAGGATTTTTTTTTTTTTTTTTCCATCTTT /3AlexF647N/	All sensors with Q_8QS_{18}
Query_Q_8QS_{33}	CGCGGCCCAGGATTTTTTTTTTTTTTTTTTTTTTTTTTTTTTTTTCCATCTTT/3AlexF647N/	All sensors with Q_8QS_{33}
Anchor_C_6CS_3	TTAGATGGTTTTCCTGGGCCGCGGGACACTCCGCCTTTTTTTT/3Bio-TEG/	All sensors with C_6CS_3
Anchor_C_7CS_3	TTAAGATGGTTTTCCTGGGCCGCGGGACACTCCGCCTTTTTTTT/3Bio-TEG/	All sensors with C_7CS_3
Anchor_C_8CS_3	TTTCCTGGGCCGCGGGACACTCCGCCTTTTTTTT/3Bio-TEG/	All sensors with C_8CS_3
CI_{mis}	TCCGCCATATAACACTGTCTG	Removes capture probe from non-target-bound sensor. Sequence has mismatch in area that binds to capture linker.
CI_{full}	TCCGCCAAATAACACTGTCTG	Removes capture probe from non-target-bound sensor. Sequence is fully complementary to its target on the capture probe.
QI	GAGTGTCCCGCGGCCCAGGA	Removes query probe from non-target-bound sensor

Table S2. The list of oligonucleotides used for detection of *EGFR* exon19 deletion mutant DNA (*EGFR*Δ_{exon_19}).

ID	Sequence: 5′-3′	Usage
Capture_ Exon 19	/5AmMC6/AG+CG+ACG+GG+AATTTGGCGGAGTGTCC	All sensors
Query_Q_8QS_{18}	CGCGGCCCAGGATTTTTTTTTTTTTTTTTTATGTTTTG/3AlexF647N/	All sensors with Q_8QS_{18}
Anchor_C_6CS_4	TTAAACATCTTTTCCTGGGCCGCGGGACACTCCGCCTTTTTTTT/3Bio-TEG/	Sensor $Q_8C_6QS_{18}CS_4$
Anchor_C_6CS_{12}	TTAAACATCTTTTTTTTTTTCCTGGGCGCGGGACACTCCGCCTTTTTTTT/3Bio-TEG/	Sensor $Q_8C_6QS_{18}CS_{12}$
Anchor_C_6CS_{19}	TTAAACATCTTTTTTTTTTTTTTTTTTTCCTGGGCCGCGGGACACTCCGCCTTTTTTTT/3Bio-TEG/	Sensor $Q_8C_6QS_{18}CS_{19}$
Anchor_C_7CS_{19}	TTAAAACATCTTTTTTTTTTTTTTTTTTTCCTGGGCCGCGGGACACTCCGCCTTTTTTTT/3Bio-TEG/	Sensor $Q_8C_7QS_{18}CS_{19}$
Anchor_C_8CS_{19}	TTACAAACATCTTTTTTTTTTTTTTTTTTTCCTGGGCCGCGGGACACTCCGCCTTTTTTTT/3Bio-TEG/	Sensor $Q_8C_8QS_{18}CS_{19}$
EGFR exon 19 del MUT_ FW	TTCCCGTCGCTATCAAGACATCTCCGAAAGCCAACAAGTAGGAC	FW and Rev strands were annealed to prepare dsDNA. FW strand was detected
EGFR exon 19 del MUT_Rev	GTCCTACTTGTTGGCTTTCGGAGATGTCTTGATAGCGACGGGAA	
EGFR exon 19 WT_FW	TTCCCGTCGCTATCAAGGAATTAAGAGAAGCAACATCTCCGAAAGCCAACAAGTAGGAC	FW and Rev strands were annealed to prepare dsDNA. FW strand was detected
EGFR exon 19 WT_Rev	GTCCTACTTGTTGGCTTTCGGAGATGTTGCTTCTCTTAATTCCTTGATAGCGACGGGAA	
CI_{20}	TCCGCCAAATTCCCGTCGCT	Removes non-target-bound capture probe
CI_{15}	ACTCCGCCAAATTCC	Removes non-target-bound capture probe
CI_{17}	ACTCCGCCATATTCCCG	Removes non-target-bound capture probe
CI_{18}	ACTCCGCCTTTTTCCCGT	Removes non-target-bound capture probe
CI_{22}	ACTCCGCCATATTCCCGTCGCT	Removes non-target-

		bound capture probe
QI	GAGTGTCCCGCGGCCCAGGA	Removes non-target-bound query probe

Table S3: The free energy (ΔG) and melting temperature (T_m) of query-target (Q-T) and query-competitor (Q-C) duplexes in different iSiMREPS sensors used for detection of miR-141.

Sensor ID	Complementary (bp)		ΔG (kcal/mol)		T_m (°C)	
	Q-T	Q-C	Q-T	Q-C	Q-T	Q-C
$Q_8C_6QS_{18}CS_3$	8	6	-13.56	-9.67	30.2	7.5
$Q_8C_6QS_{33}CS_3$	8	6	-13.56	-9.67	30.2	7.5
$Q_8C_7QS_{18}CS_3$	8	7	-13.56	-11.62	30.2	18.1
$Q_8C_7QS_{33}CS_3$	8	7	-13.56	-11.62	30.2	18.1

Note: ΔG and T_m were calculated using IDT oligo analyzer (https://www.idtdna.com/calc/analyzer) using the complementary segments that form the duplex. All calculations were carried out at 25˚C with 1μM oligo concentrations, 600 mM Na^+ ions.

Table S4: The free energy (ΔG) and melting temperature (T_m) of query-target (Q-T) and query-competitor (Q-C) duplexes for different iSiMREPS sensors used for detection of *EGFR* exon 19 deletion mutant DNA (*EGFR*Δ_{exon_19}).

Sensor ID	Complementary (bp)		ΔG (kcal/mol)		T_m (°C)	
	Q-T	Q-C	Q-T	Q-C	Q-T	Q-C
$Q_8C_6QS_{18}CS_4$	8	6	-11.7	-9.1	23.9	0
$Q_8C_6QS_{18}CS_{12}$	8	6	-11.7	-9.1	23.9	0
$Q_8C_6QS_{18}CS_{19}$	8	6	-11.7	-9.1	23.9	0
$Q_8C_7QS_{18}CS_4$	8	7	-11.7	-10.6	23.9	11.7
$Q_8C_8QS_{18}CS_4$	8	8	-11.7	-11.7	23.9	23.9

Note: ΔG was predicted using NUPACK(Caltech: , 2007; Zadeh et al., 2011) and T_m was calculated using IDT oligo analyzer (https://www.idtdna.com/calc/analyzer). The single stranded regions (spacers) flanking the complementary segments of query, target and competitor probe were considered to calculate ΔG using NUPACK(Caltech: , 2007; Zadeh et al., 2011), but only complementary segments were considered to calculate T_m using IDT oligo analyzer. All calculations were carried out at 25˚C with 1μM oligo concentrations, 600 mM Na^+ ions.

Table S5. The criteria for manually selecting traces from prism-based TIRF experiments.

Criterion	**Rationale**
Trace must have acceptor signal	Prevents traces with a bleached acceptor or no query probe from being included
Trace must not have multistep transitions	This convolutes the signal and makes it harder to separate genuine FRET transitions from off-target noise
Movies with signal that drifts into the baseline will not be accepted	Data from these movies is less trustworthy because of worsening S/N creating FRET states that can't be distinguished from noise
Unusually low High FRET or unusually high Low FRET values and S/N weak enough that it dips into baseline area	Traces with these features will be more susceptible to incorrect assignment of FRET states in HMM modeling
If there were multiple segments, the longest one was chosen and if they were of comparable lengths, the one with better S/N or clearer transitions was chosen.	This prevents the kinetic data from being too weighted or biased by a few traces with a large number of transitions.
If the final signal in a chosen segment is low FRET, it is only included if there is an acceptor signal after it.	This prevents signals after photobleaching of the acceptor from tainting the kinetic data
Traces with no distinction between baseline and signal are rejected	A static signal and an unusually intense baseline cannot be distinguished

Table S6. Acquisition parameters and default kinetic filtering criteria for different iSiMREPS sensors, with and without formamide, for detecting miR-141.

Parameter	Default	0%F 10s	0%F 30s	5%F	10%F	15%F	20%F
Frames	1-166	1-166	1-500	1-166	1-166	1-166	1-166
Exposure Time (s)	0.06	0.06	0.06	0.06	0.06	0.06	0.06
Intensity Threshold	200	200	200	200	200	200	200
Max Intensity	Inf	Inf	Inf	Inf	Inf	Inf	Inf
S/N Event Threshold	2	2	2	2	2	2	2
S/N Trace Threshold	3.5	4.5	3.8	4.5	3.4	3.4	1.4
Minimum N_{b+d}	5	2	4	4	3	5	6
Maximum N_{b+d}	Inf	Inf	Inf	Inf	Inf	Inf	Inf
Minimum $\tau_{on,\ median}$ (s)	0.06	0.24	0.18	0.06	0.06	0.06	0.06
Maximum $\tau_{on,\ median}$ (s)	10	9.9	19.98	7.38	7.44	1.38	2.7
Minimum $\tau_{off,\ median}$ (s)	0.06	0.12	0.18	0.06	0.06	0.06	0.06
Maximum $\tau_{off,\ median}$ (s)	0.9	3.3	6.06	2.82	2.1	1.2	0.6
Maximum $\tau_{on,\ event}$ (s)	5	Inf	22.5	8.82	3.96	9.78	9.54
Maximum $\tau_{off,\ event}$ (s)	4	Inf	15	5	4	4	2.34
Minimum $\tau_{on,}$ CV	Inf	Inf	Inf	Inf	Inf	Inf	Inf
Maximum $\tau_{on,}$ CV	Inf	Inf	Inf	Inf	Inf	Inf	Inf

Note: All experiments other than the ones indicated specifically in this table use the settings listed under "default". The formamide variance filtering settings shown here represent data from 1 trial and were obtained using the SiMREPS kinetic parameters optimizer, which gives a starting point of filtering settings to maximize counts and minimize false positives using real and control data sets. The exact filtering settings vary from day to day for formamide experiments, as they were selected using the optimizer to gauge each condition's best possible performance. The τ_{on} and τ_{off} indicate target bound (high-FRET) and non-target-bound (low-FRET) states, respectively.

Table S7. Acquisition parameters and default kinetic filtering criteria for different iSiMREPS sensors with and without formamide for detecting *EGFR* exon 19 deletion mutant DNA (*EGFR*Δ_{exon_19}).

Sensors	$Q_8C_6QS_{18}CS_4$	$Q_8C_6QS_{18}CS_{12}$	$Q_8C_6QS_{18}CS_{19}$	$Q_8C_7QS_{18}CS_{19}$	$Q_8C_8QS_{18}CS_{19}$	$Q_8C_6QS_{18}CS_{19}$	$Q_8C_6QS_{18}CS_{19}$	$Q_8C_6QS_{18}CS_{19}$
Formamide (%)	0	0	0	0	0	0	5-10	15-20
Start-to-end frame	1-200	1-200	1-200	1-200	1-200	1-100	1-100	1-100
Exposure time per frame (s)	0.1	0.1	0.1	0.1	0.1	0.1	0.1	0.1
Acquisition time (s)	20	20	20	20	20	10	10	10
Intensity threshold per trace	500	500	500	500	500	500	500	500
S/N threshold per event	1.5	1.5	1.5	1.5	1.5	1.5	1.5	1.5
S/N threshold per trace	1.7	3.7	2.6	2.9	4.5	1.5	1.5	1.5
Minimum N_{b+d}	5	5	5	5	5	5	6	8
Maximum N_{b+d}	Inf	Inf	Inf	Inf	Inf	Inf	Inf	Inf
Minimum $\tau_{on,\ median}$ (s)	0.1	0.3	0.1	0.1	0.1	0.1	0.1	0.1
Maximum $\tau_{on,\ median}$ (s)	10	10	10	10	10	6	6	6
Minimum $\tau_{off,\ median}$ (s)	0.1	0.1	0.1	0.1	0.1	0.1	0.1	0.1
Maximum $\tau_{off,\ median}$ (s)	10	10	10	10	10	6	6	6
Minimum $\tau_{on,}$ CV	Inf	Inf	Inf	Inf	Inf	Inf	Inf	Inf
Maximum $\tau_{on,}$ CV	Inf	Inf	Inf	Inf	Inf	Inf	Inf	Inf
Maximum $\tau_{on,\ event}$ (s)	12	12	12	12	12	8	8	8
Maximum $\tau_{off,\ event}$ (s)	12	12	12	12	12	8	8	8
Maximum $I_{low\ FRET\ state}$ per trace	Inf	Inf	Inf	Inf	Inf	Inf	Inf	Inf
Number of intensity states	2	2	2	2	2	2	2	2
Ignore post photobleaching (s)	12	12	12	12	12	8	8	8

Note: The default kinetic filtering criteria was determined by our newly developed machine learning based SiMREPS optimizer, which used data sets with multiple FOVs (e.g.., ≥ 10) from at least three independent experiments with and without the target as training data. For each individual experiment, the default kinetic filtering criteria were optimized slightly to minimize false positives in the negative control without rejecting true positive counts in the positive sample. The τ_{on} and τ_{off} indicate target bound (high-FRET) and non-target-bound (low-FRET) states, respectively.

Table S8: Calculation of specificity for detecting *EGFR* exon 19 deletion mutant DNA (*EGFR*Δ_{exon_19}).

Mutant allele (%)	MUT (fM)	WT (nM)	C_{WT}/C_{MUT}	Counts ± s.d. in MUT +WT (n = 4)	Counts ± s.d. in WT-only (n = 4)	Specificity (%) = $[1 - \frac{FP}{TP \times (C_{WT}/C_{MUT})}] \times 100$
0.001	500	50	10^5	4.0 ± 1.2	1.2 ± 0.3	99.9996
0.0001	500	500	10^6	3.9 ± 0.7	1.3 ± 0.3	99.9999

3. Supplementary Figures

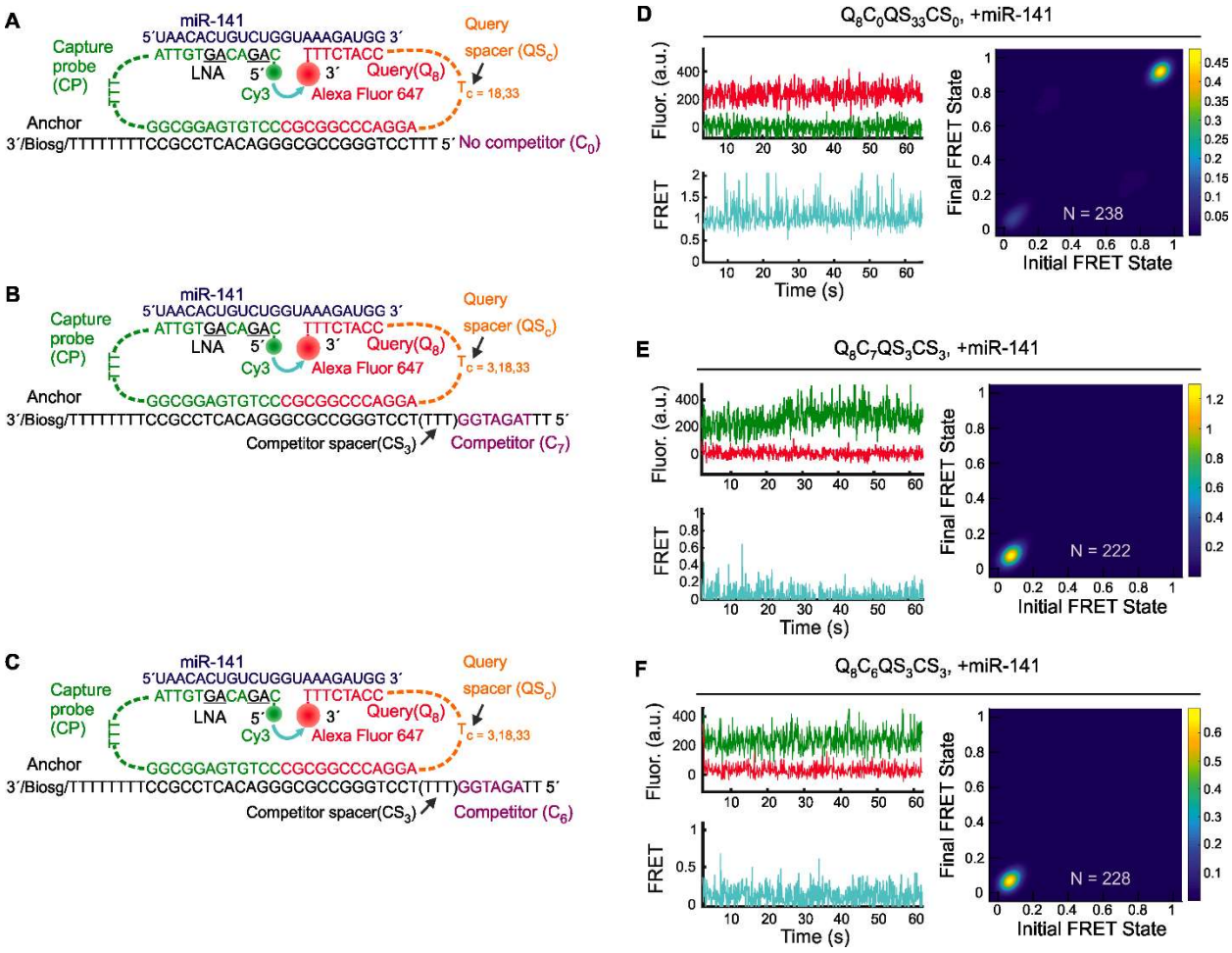

Fig. S1. Design and optimization of iSiMREPS sensors for detection of miR-141. (**A**) iSiMREPS sensor designs without any competitor sequence that differ only in the length of query spacer (i.e., 18 and 33 nt). (**B**) Sensor designs that contain a 7-nt competitor sequence that can interact with the query probe and vary in query spacer length (i.e., 3, 18 and 33 nt). (**C**) These iSiMREPS sensors contain a 6-nt competitor sequence and differ in the spacer lengths in the query probe. (**D-F**) Single-molecule kinetic traces, FRET signal, and TODP plots for the sensor $Q_8C_0QS_{18}CS_0$ (**D**), $Q_8C_7QS_3CS_3$ (**E**), and $Q_8C_6QS_3CS_3$ (**F**). All experiments were performed using preassembled anchor, capture, query and miR141 target at ~100 pM concentration and imaged under prism-TIRF microscopy. N represents number of molecules.

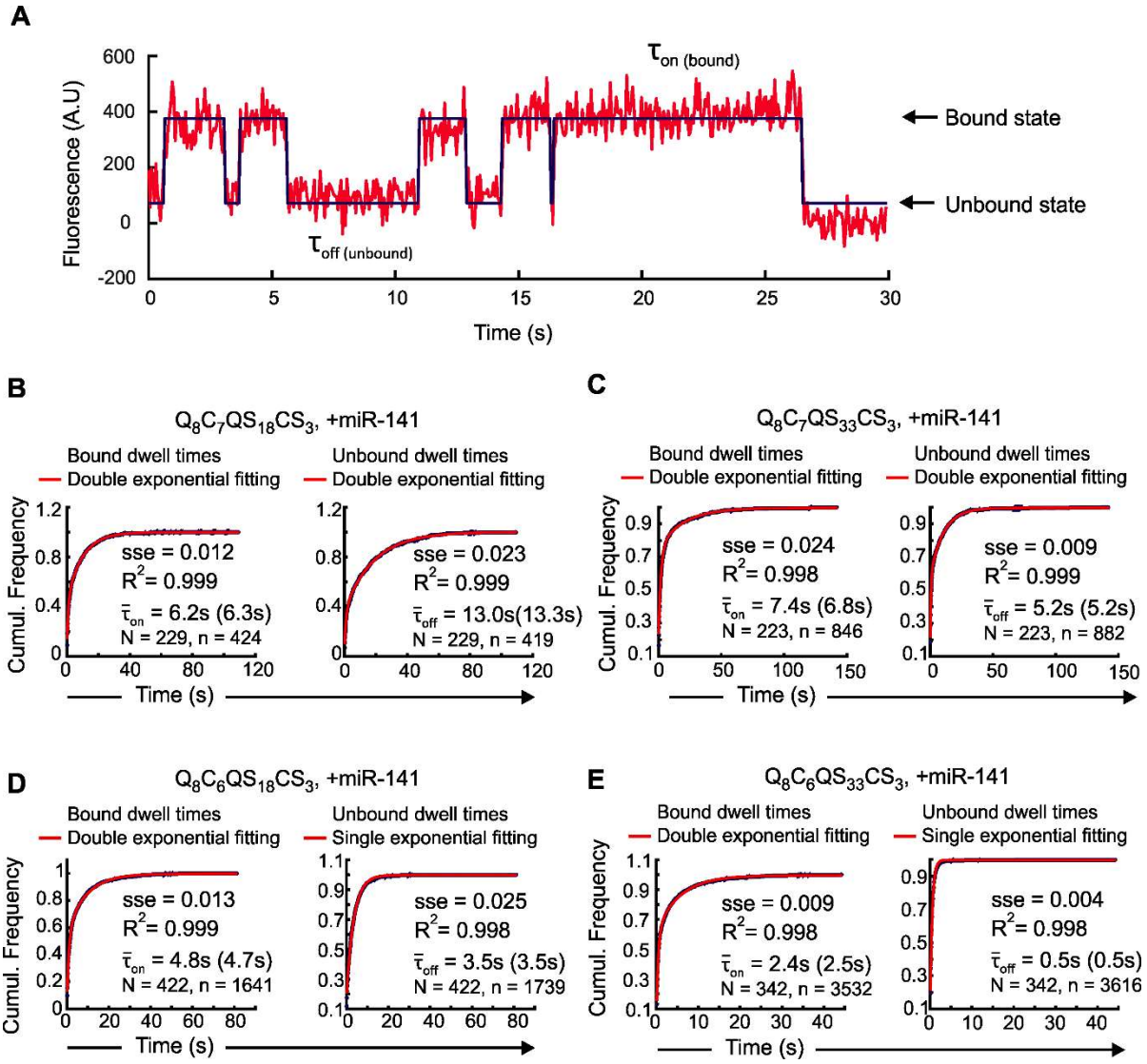

Fig. S2. Representative single molecule kinetic trace and estimation of average dwell times of FRET states for different iSiMREPS sensors for detecting miR-141. (**A**) Representative intensity-time trace fitted with tan HMM to extract the dwell times of miR-141 target bound ($\bar{\tau}_{on}$) and unbound states ($\bar{\tau}_{off}$). (**B-E**) Exponential fitting to dwell time cumulative frequency for miR-141 target bound (high-FERT) ($\bar{\tau}_{on}$) and non-target-bound (low-FRET) ($\bar{\tau}_{off}$) states for various sensors. All experiments were performed without formamide in the imaging buffer. Single exponential fitting was chosen when sum squared error (sse) <0.05 and R^2 > 0.98 and double exponential fitting was used otherwise. The time listed reflects the dwell time calculated from the best-fit curve using all accepted traces, and the time in parenthesis is the reported average when the data was split into 3 populations and is the one seen in the main text. The 'N' represents number of accepted traces, and 'n' represents the total number of dwell time events used for the fitting.

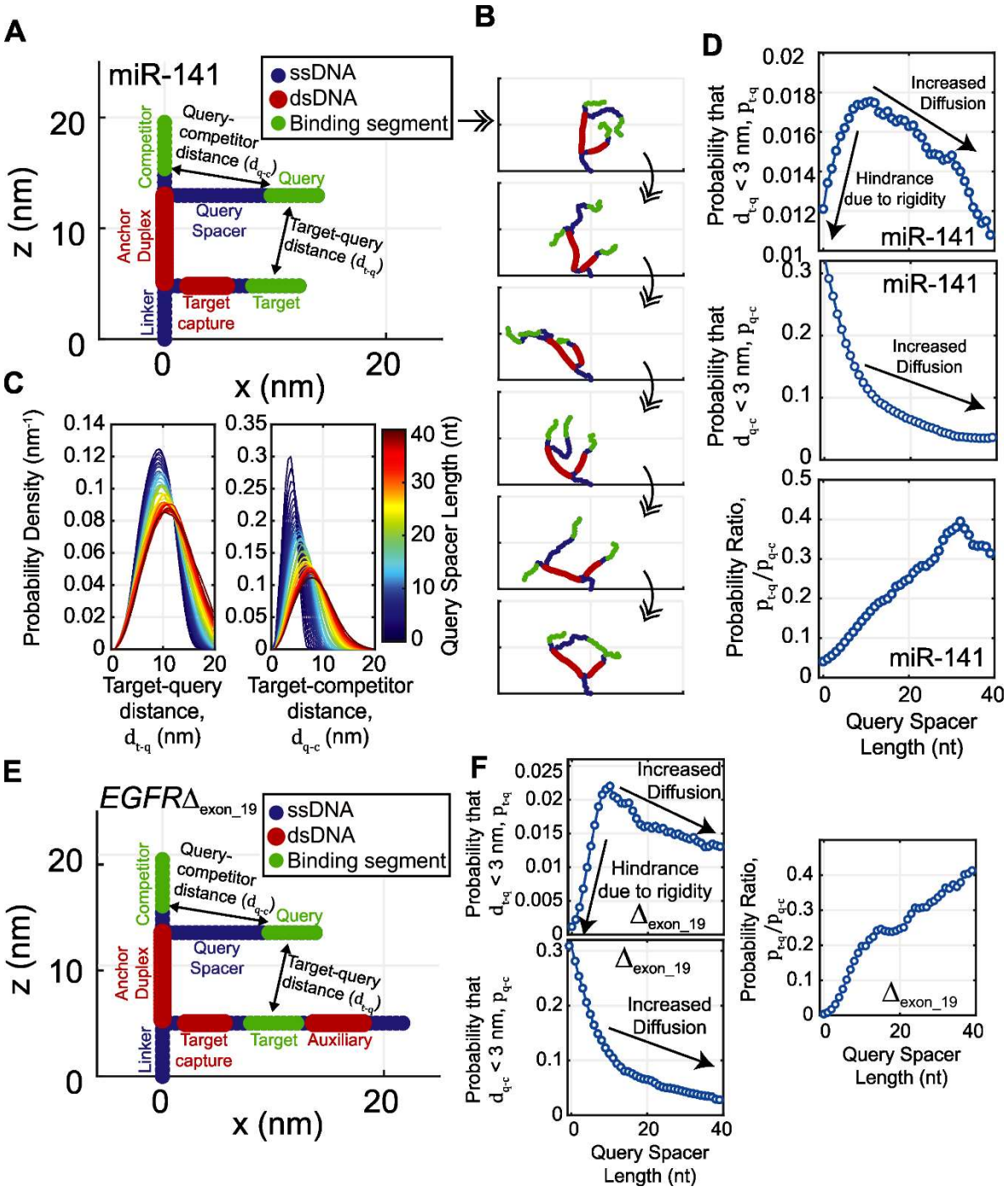

Fig. S3. Simulations support finding that iSiMREPS kinetics scale non-monotonically with query spacer length. (**A**) Initialized simulated iSiMREPS construct with labels showing the three main regions of the probe (anchor, query, and target) as well as the distances between the target and query segments (d_{t-q}) and the query and competitor segments (d_{q-c}) for the miR-141 construct. All points are represented as

circles with color denoted by polymer type as shown in the legend. (**B**) Six representative snapshots of a 2D version of the Monte Carlo simulation method, separated by at least 10,000 iterations each. (**C**) Probability density functions of d_{t-q} for simulations with query spacers lengths (depicted by color) ranging in length from 0 nt to 39 nt. (**D**) Three plots are shown. The top plot shows the probability (denoted p_{t-q}) that d_{t-q} is less than a close contact cutoff of 3 nm, as measured from the cumulative output of the Monte Carlo simulation, as a function of the query spacer length. The middle plot is similar, but for d_{q-c}. The bottom plot shows the ratio p_{t-q}/p_{q-c}. Because the activation energy for base pairing should be largely independent of spacer length and is also expected to be the rate-limiting step due to the high rate of diffusion, the strand association rate should scale linearly with p_{t-q}. Arrows in the top plot show that there are two roughly linear trend regimes. At query spacer lengths shorter than 9 nt, decreasing the spacer length decreases p_{t-q} by what we expect is a hindrance imposed by the long, stiff anchor duplex. In this regime, it is expected that this hindrance will also increase the rate of unbinding. In contrast, p_{q-c} decreases monotonically with increasing spacer length. This finding is consistent with the conformational rigidity model, as there are no dsDNA regions separating the competitor and query segments. At spacer lengths exceeding ~10 nt, increasing the spacer length mildly decreases p_{t-q} due to what we expect is an increased radius of diffusion. This trend is seen for p_{q-c} across the entire range of spacer lengths tested. However, while both p_{t-q} and p_{q-c} decrease monotonically with long spacer lengths, the ratio p_{t-q}/p_{q-c} increases monotonically across the entire range, suggesting that increasing spacer length monotonically increases the preference for the target's association with the target over the competitor. These findings hold true for cutoffs that are reasonably larger or smaller than 3 nm (not shown). Notably, this simulation method is limited in that it does not account for long-range repulsive interactions between non-neighboring regions of the probe. We expect that if we did incorporate such long-range interactions, different branches of the iSiMREPS probe would be further repelled by each other, potentially steepening the correlation observed in the long-spacer length regime. (**E**) Initialized simulated iSiMREPS *EGFR* exon 19 deletion mutant DNA (*EGFR*Δ_{exon_19}) construct with labels showing the three main regions of the probe (anchor, query, and target + auxiliary complex), like that shown in A. (**F**) Results for a simulation of the *EGFR*Δ_{exon_19}design show similar trends to those shown in D.

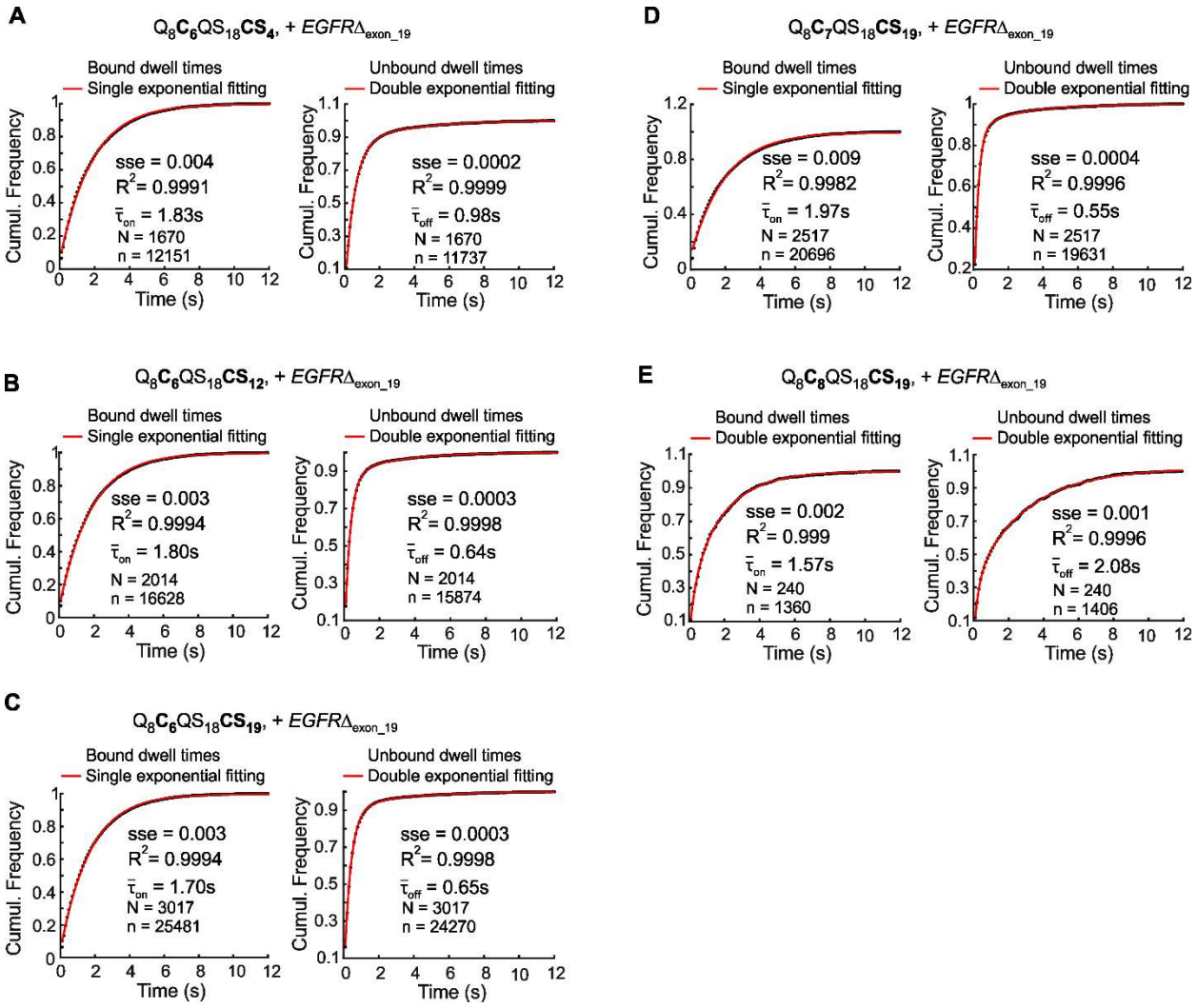

Fig. S4. Estimation of average dwell times smFRET states for different iSiMREPS sensors for detecting *EGFR* exon 19 deletion mutant DNA (*EGFR*Δexon_19). (**A-E**) Calculation of the average dwell time for the target bound (high-FRET) ($\bar{\tau}_{on}$) and non-target-bound (low-FRET) ($\bar{\tau}_{off}$) states for different iSiMREPS sensors for detecting *EGFR*Δexon_19. All experiments were performed without formamide in the imaging buffer. For all the sensors except the one with an 8-nt competitor, the target bound state dwell times were fitted with a single exponential. Single exponential fitting was chosen when sum squared error (sse) <0.08 and R^2 > 0.96, and double exponentials were used otherwise. All non-target-bound dwell times were fitted with a double exponential. All data is from 1 of 3 independent experiments. The 'N' represents number of accepted traces, and 'n' represents the total number of dwell time events used for the fitting.

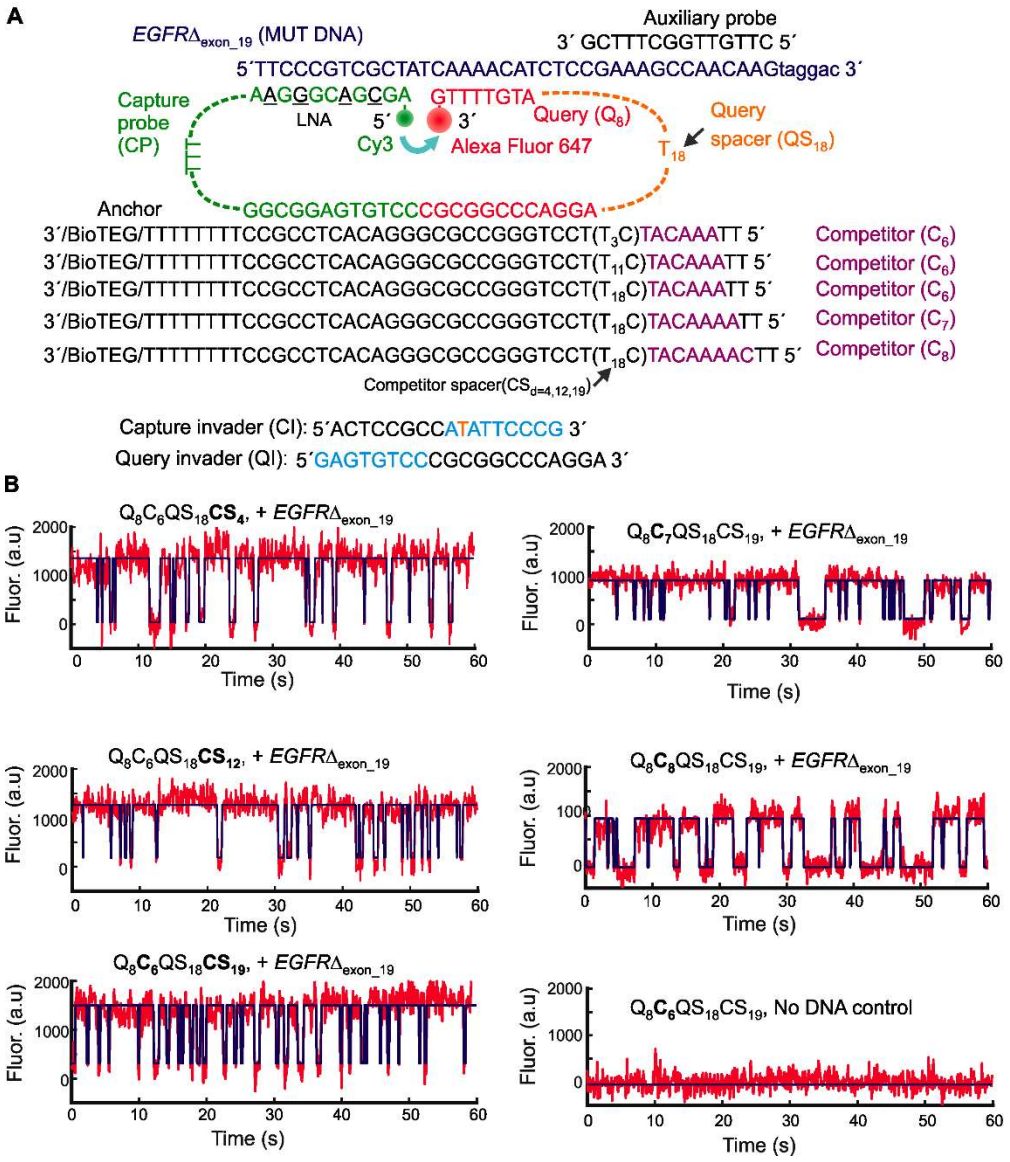

Fig. S5. Schematic of different iSiMREPS sensors and representative single molecule kinetic traces in the presence of *EGFR* exon 19 deletion mutant DNA (*EGFR*Δexon_19). (**A**) Designs of iSiMREPS sensors for detecting *EGFR*Δexon_19with various competitor spacer (CS) and competitor (C) lengths. (**B**) Representative single-molecule kinetic traces (red) for different iSiMREPS sensors with or without *EGFR*Δexon_19 with an idealized hidden Markov model (HMM) fit (blue). All experiments were performed using 10 nM preassembled sensors consisting of anchor, capture and query probes, and 10 pM *EGFR*Δexon_19 forward strand. Imaging was done in 4x PBS (pH 7.4) at room temperature under an objective-type-TIRF microscope. The donor fluorophore (Cy3) was excited at 532 nm and the acceptor fluorescence (Alexa Fluor 647) was recorded as FRET signal.

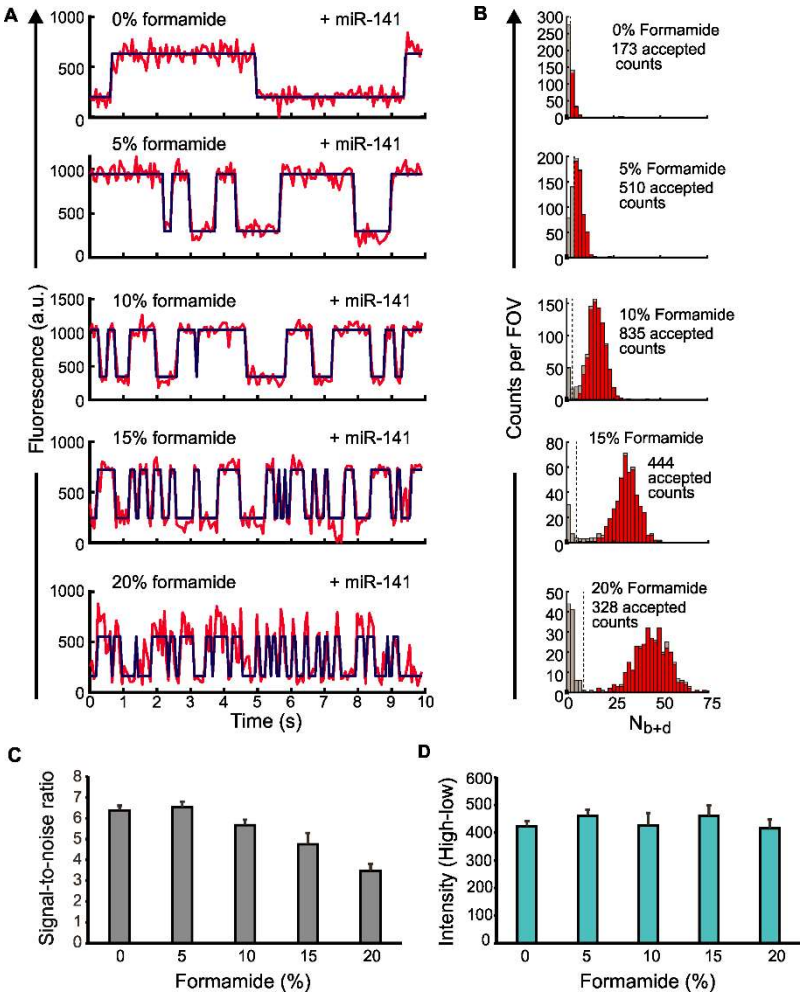

Fig. S6. Effects of formamide on the iSiMREPS sensor for detecting miR-141. (**A**) Representative traces for the $Q_8C_6QS_{18}CS_3$ miR-141 sensor at 0, 5, 10, 15, and 20% v/v formamide. The signal is in red while the idealized trace obtained from hidden Markov model (HMM) fitting is in blue. (**B**) Histograms from 1 of 3 independent experiments for each formamide condition that show the distribution of N_{b+d} among the accepted traces. These histograms reflect the distribution after application of filters for parameters such as signal-to-noise, intensity, and min and max average lifetimes. The red bars represent traces accepted while the grey bars represent traces rejected. (**C**) The average intensity difference between the high and low FRET states in the idealized hidden Markov model for each formamide condition. (**D**) The average signal-to-noise for a trace for each formamide condition. For all experiments shown, sensors were assembled at 200 nM in the presence of 5 nM miR-141. The pre-assembled sensors were then diluted it 1,000-fold and added to the surface. Imaging was performed in 4× PBS at pH 7.4. All data are presented as mean ± s.d. of 3 independent experiments.

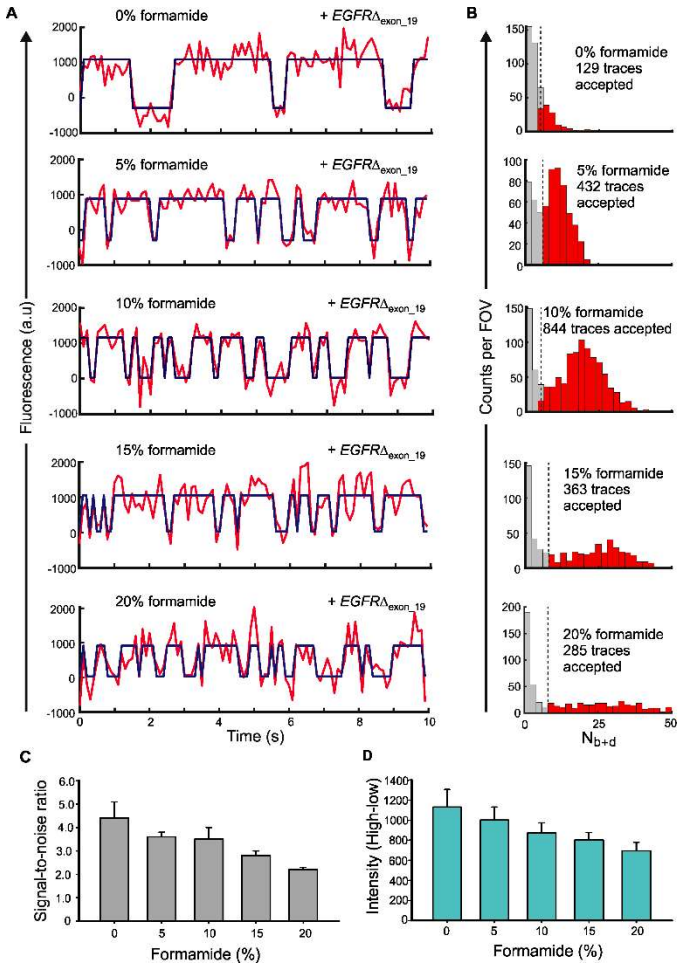

Fig. S7. Effects of formamide on the iSiMREPS sensor for detecting *EGFR* exon 19 deletion mutant DNA (*EGFR*Δ_{exon_19}). (**A**) Representative single-molecule kinetic traces (red) with an idealized hidden Markov model (HMM) fit (blue) of the $Q_8C_6QS_{18}CS_{19}$ sensor for detecting *EGFR*Δ_{exon_19} at different formamide conditions. (**B**) Histograms of the number of candidate molecules per field-of-view (FOV) showing a given number of binding and dissociation events (N_{b+d}) after applying thresholds for FRET intensity, signal-to-noise, and dwell times of target-bound and non-target-bound states for each formamide condition. Red bars represent accepted traces while grey bars represent rejected traces. (**C, D**) The average signal-to-noise ratio (**C**), and difference in intensity of high- and low-FRET states (**D**) of the accepted traces for each formamide condition. All experiments were performed using 10 nM preassembled sensor consisting of anchor strand, capture and query probes, and 10 pM forward strands of *EGFR*Δ_{exon_19}. Imaging was performed in 4x PBS (pH 7.4) at ambient room temperature under an objective-TIRF microscope. All data are presented as mean ± s.d. of 3 independent experiments.

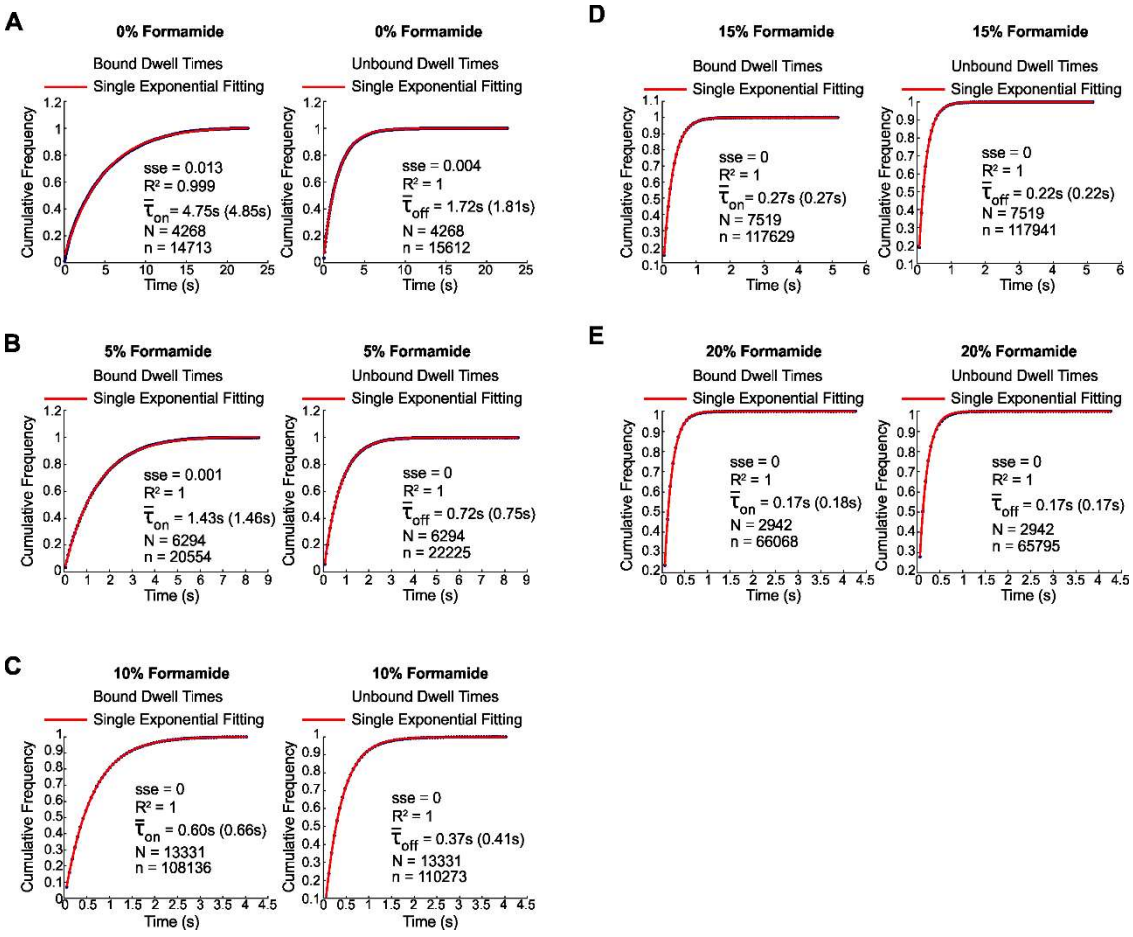

Fig. S8. Estimation of average dwell times of FRET states with the variation of formamide concentration using optimized iSiMREPS sensor for detecting miR-141. (**A-E**) Calculation of the average dwell time of high-($\bar{\tau}_{on}$) and low-FRET ($\bar{\tau}_{off}$) states for miR-141 for each formamide condition, obtained by fitting an exponential decay function to the cumulative frequency. Single exponential fits were used for all experiments depicted here as all had a sum squared error (sse) <0.05 and R^2 > 0.98. These curves represent the dwell times obtained in 1 of the 3 independent experiments conducted for each condition and the time in parentheses is the average time obtained from these independent experiments. The 'N' represents number of accepted traces, and 'n' represents the total number of apparent dwell time events in the accepted traces that used for the fitting. Experiments without formamide used a 30 s window to ensure accurate dwell times were obtained while a 10 s window was sufficient for all other conditions. The N value listed is the number of bound and unbound events in the accepted traces that contributed to the fitting.

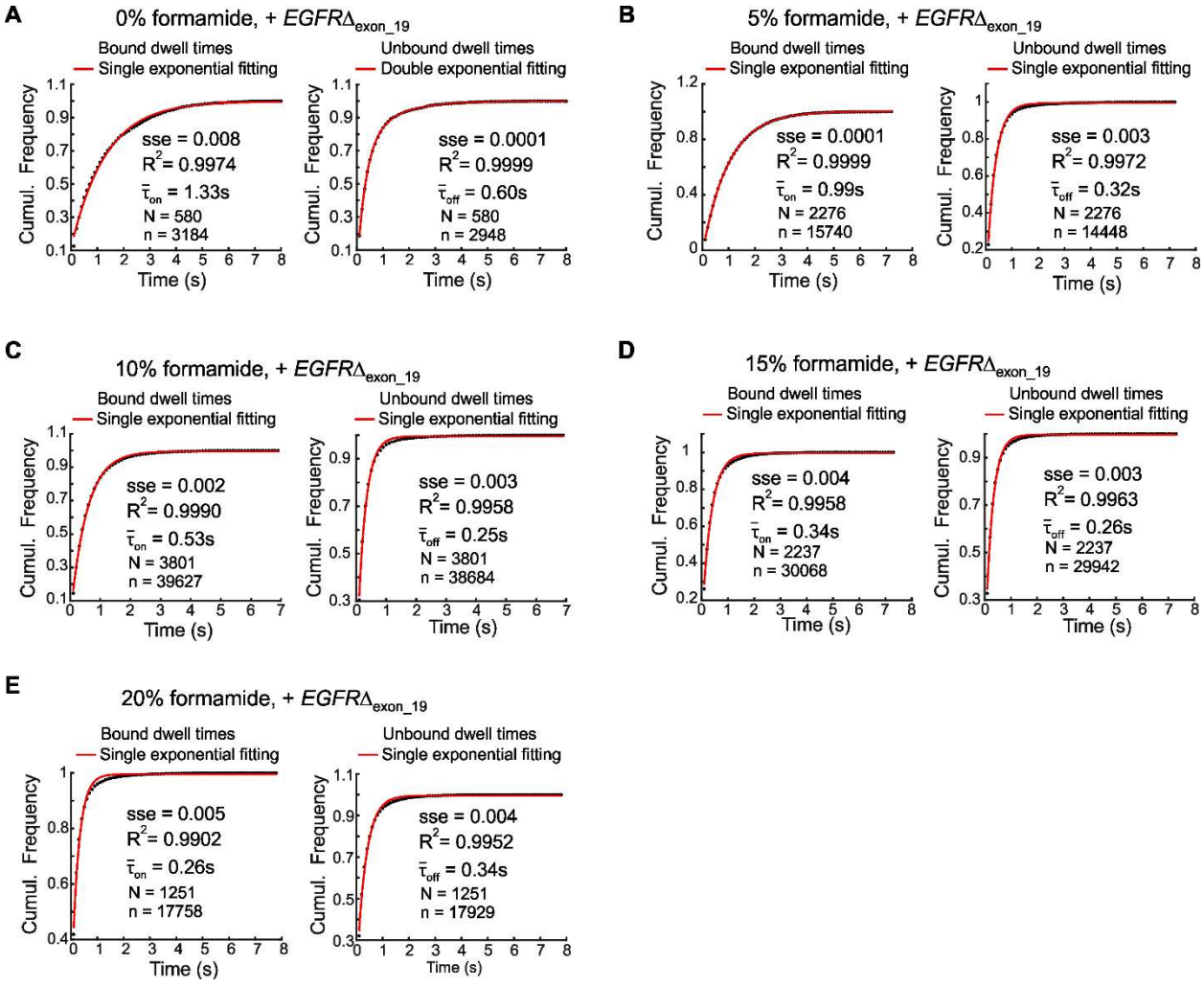

Fig. S9. Estimation of average dwell times of FRET states with the variation of formamide concentration using optimized iSiMREPS sensor for detecting *EGFR* exon 19 deletion mutant DNA (*EGFR*Δexon_19). **(A-E)** Calculation of the average dwell time for the target bound (high-FRET) ($\bar{\tau}_{on}$) and non-target-bound (low-FRET) ($\bar{\tau}_{off}$) states of the sensor $Q_8C_6QS_{18}CS_{19}$ for detecting *EGFR*Δexon_19 at different formamide concentrations (0-20% v/v) by fitting an exponential decay function to the cumulative frequency. Both target bound and non-target-bound dwell times for all conditions except 0% formamide were fitted with a single exponential decay function. Single exponential fitting was chosen when sum squared error (sse) <0.08 and R^2 > 0.96 and double exponential was used otherwise. All data are from 1 of 3 independent experiments. The 'N' represents number of accepted traces, and 'n' represents the total number of apparent dwell time events in the accepted traces that used for the fitting.

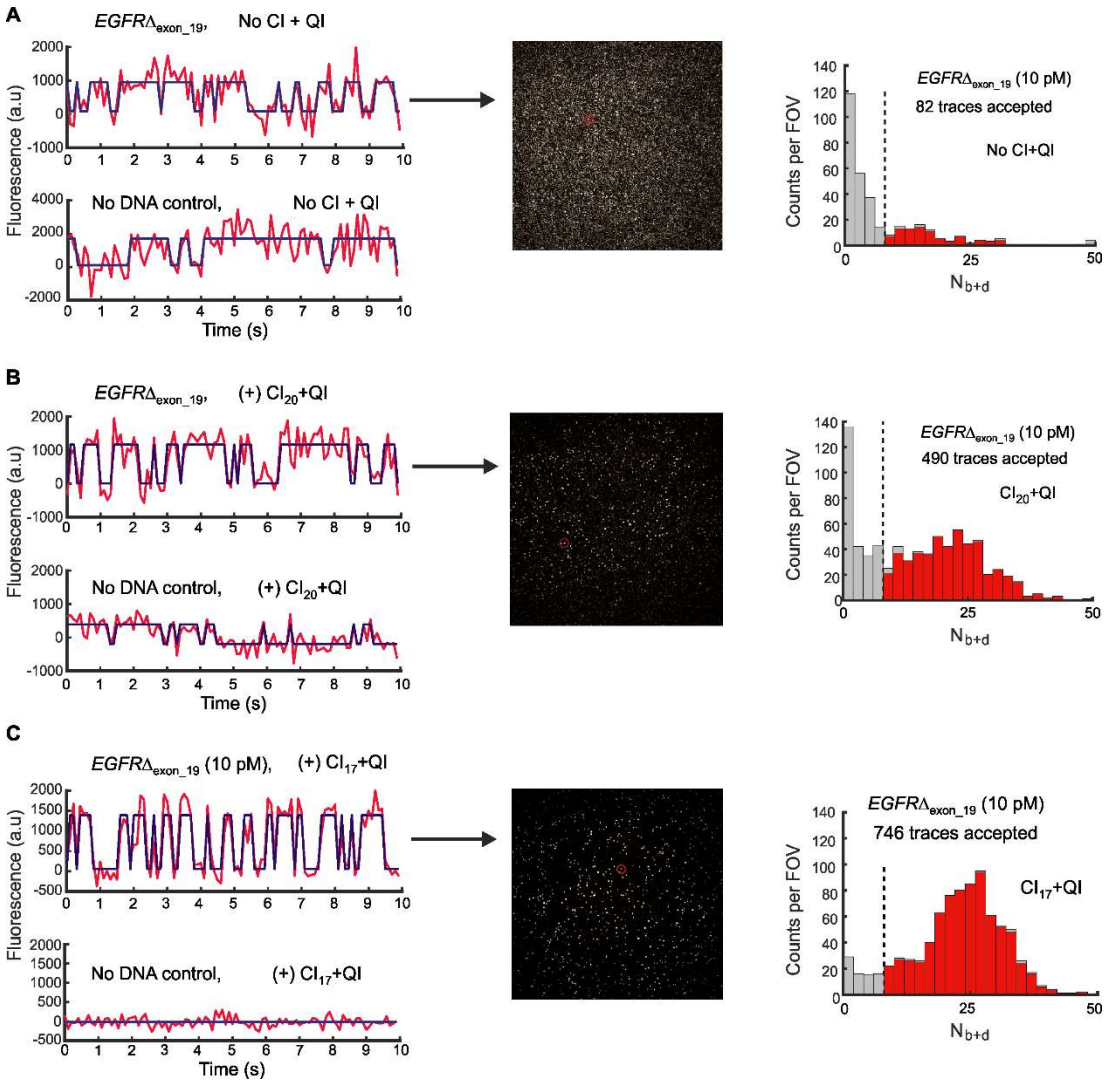

Fig. S10. Effect of different invaders on the background signals to detect *EGFR* exon 19 deletion mutant DNA (*EGFR*Δexon_19). (**A-C**) Representative single-molecule kinetic traces, images of a field-of-view (FOV) and histograms of the number of candidate molecules per FOV showing a given number of binding and dissociation events (N_{b+d}) detected in 10 s per FOV, after applying thresholds for FRET intensity, S/N, and lifetimes of bound and unbound states without invaders (**A**), with invaders CI_{20}+QI (**B**), and with invaders CI_{17}+QI (**C**) in the presence and absence of *EGFR*Δexon_19 target (see Figure 5A for invaders sequences). All experiments were performed using 0.2 mg/mL streptavidin (incubation: 10 min), 10 nM sensor (incubation: 30 min), 10 pM forward strands of *EGFR*Δexon_19 (incubation: 90 min), 1 μM invaders (incubation: 20 min). Objective-TIRF imaging was performed in the presence of 10 % v/v formamide in the imaging buffer. All data are presented as the mean ± s.d. of n = independent experiments.

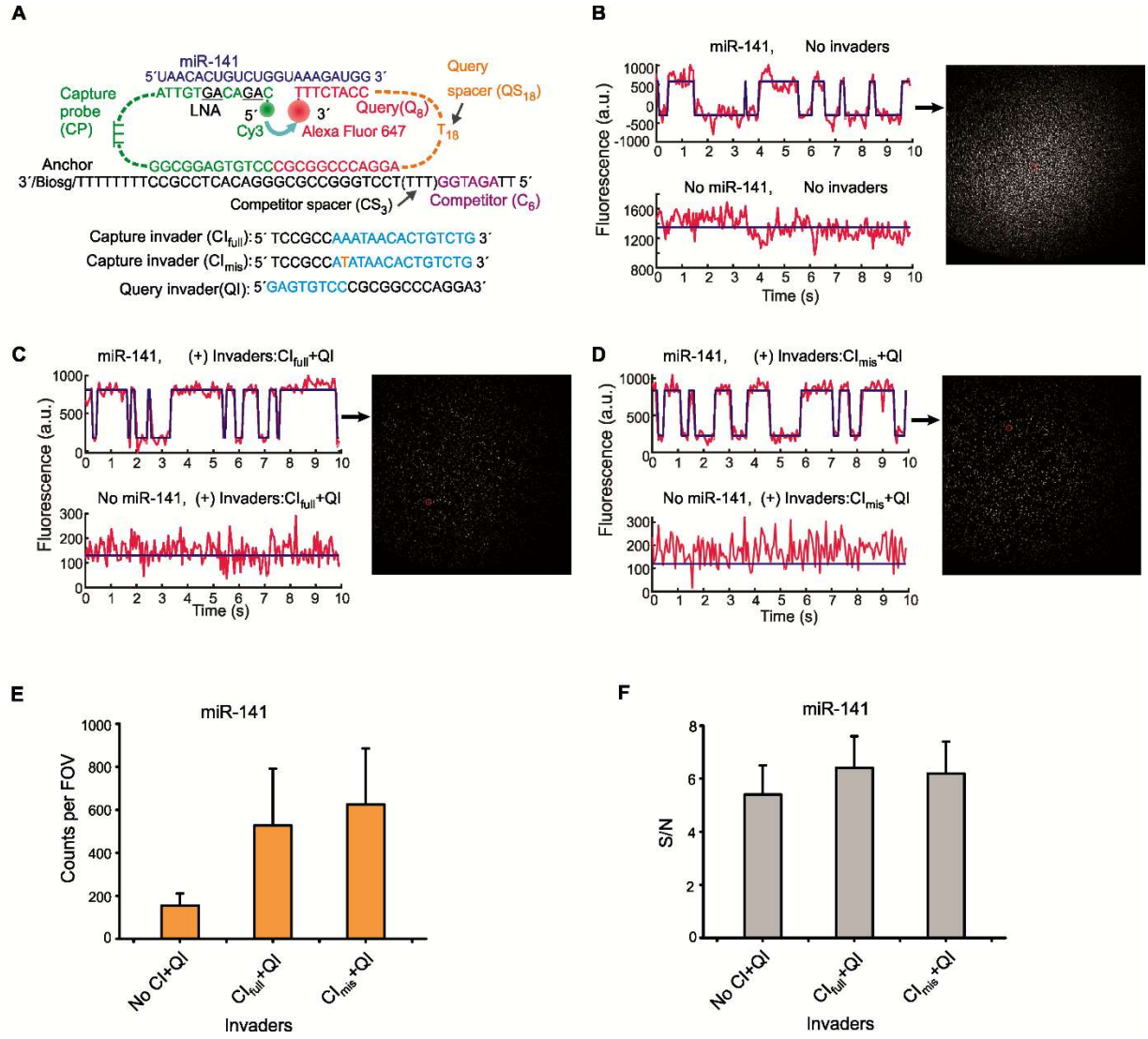

Fig. S11. Schematic of the design of iSiMREPS sensor for detecting miR-141 and representative single molecule kinetic traces in the presence and absence of different invaders. (**A**) Design of the optimized miR-141 sensor and different invaders tested. (**B-D**) Representative single-molecule kinetic traces and images of a FOV without invaders (**B**), with invaders CI_{full}+QI (**C**), and with invaders CI_{mis}+QI (**D**) in the presence and absence of miR-141. (**E**) Number of accepted counts per FOV in the presence of miR-141 after application of different capture invaders. (**F**) S/N ratio in the candidate target bound molecules after application of different capture invaders. Overall application of invaders improved the background signals as well the signal-to-noise ratio of single molecule traces as well as accepted counts compared to without invaders application. For all experiments shown, sensors were assembled at 200 nM in the presence of 5 nM miR-141. The pre-assembled sensors were then diluted it 1,000-fold and added to the surface. Imaging was performed in 4× PBS at pH 7.4. All data are presented as the mean ± s.d. of n = independent experiments.

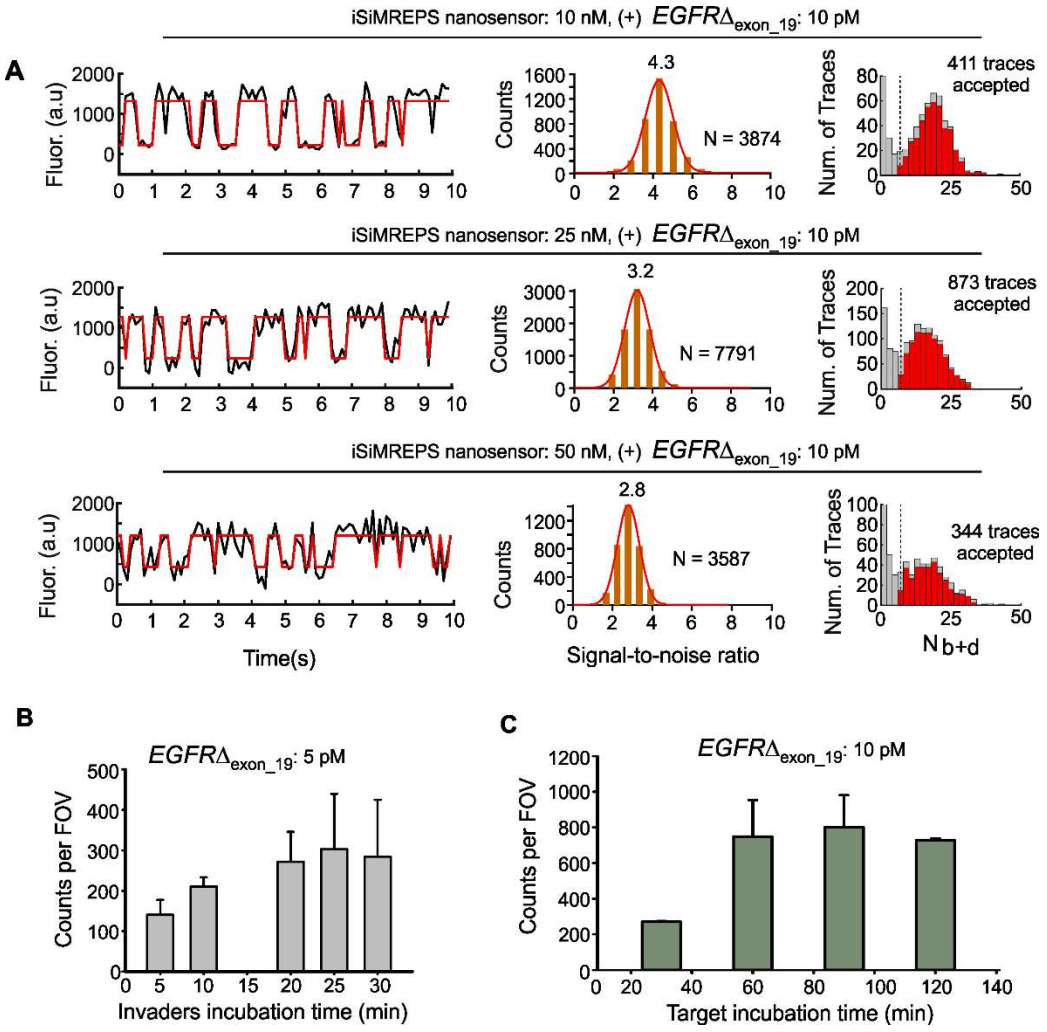

Fig. S12. Optimization of iSiMREPS assay conditions to enhance sensitivity for detection of *EGFR* exon 19 deletion mutant DNA (*EGFR*Δ_{exon_19}). (A) Effect of sensor concentration on signal-to-noise ratio (S/N) and the number of accepted traces. The experiment was performed using 10, 25, and 50 nM sensor (incubation: 30 min), 10 pM forward strands of *EGFR*Δ_{exon_19} (incubation: 90 min), and 2.5 μM invaders (incubation: 20 min). (B) Effect of invaders incubation times on accepted traces. The experiment was performed using 25 nM sensor (incubation: 30 min), 5 pM forward strands of *EGFR*Δ_{exon_19} (incubation: 90 min), and 2.5 μM invaders (incubation: 5, 10, 20, 25, 30 min). (C) Effect of target incubation times on accepted counts. This experiment was performed using 25 nM sensor (incubation: 30 min), 10 pM forward strands of *EGFR*Δ_{exon_19} (incubation: 30, 60, 90, and 120 min), and 2.5 μM invaders (incubation: 25 min). All experiments were performed using the sensor $Q_8C_6QS_{18}CS_{19}$. All data are presented as mean ± s.d. of 2 independent experiments.

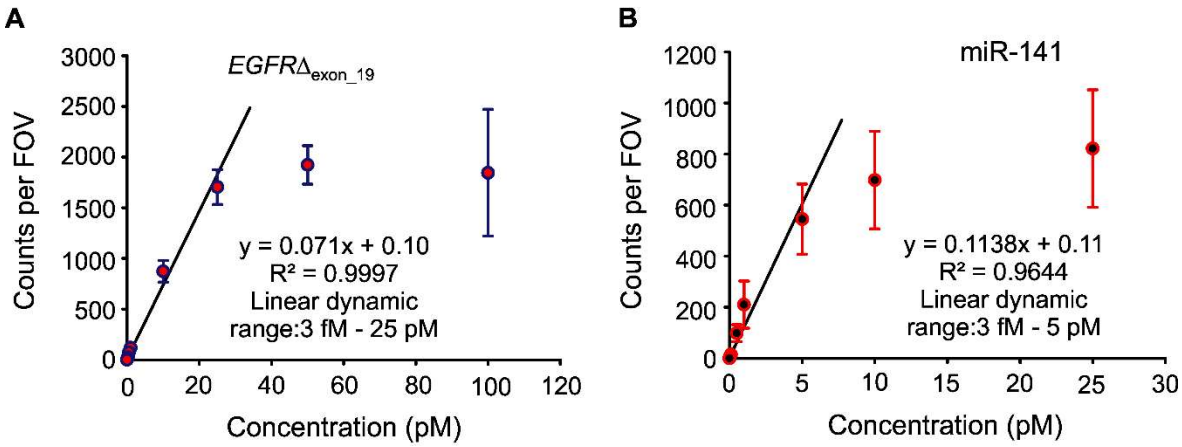

Fig. S13. Standard curves for miR-141 and *EGFR* exon 19 deletion mutant DNA (*EGFR*Δ_{exon_19}). (**A**) Standard curves showing the linear dynamic range for detection of *EGFR*Δ_{exon_19} dsDNA. The experiments were performed using a glass coverslip passivated with biotin-PEG: m-PEG at a 1:100 ratio, 0.5 mg/mL streptavidin incubation for 10 min, 25 nM sensor incubation for 30 min, 1.96 fM to 100 pM *EGFR*Δ_{exon_19}dsDNA incubation for 90 min, 2.5 µM invaders (CI_{17} + QI) incubation for 20 min, and 10% v/v formamide. All data are presented as mean ± s.d., where n ≥ 3 independent experiments. iSiMREPS showed a linear dynamic range of approximately 3 fM - 25 pM for detecting *EGFR*Δ_{exon_19} which is approximately 3.9 orders of magnitude. (**B**) Standard curves showing linear dynamic range for detection of miR-141. The experiments were performed using a glass coverslip passivated with biotin-PEG: m-PEG at a ratio of 1:100, then incubated with 0.2 mg/mL streptavidin for 10 min, 10 nM sensor for 30 min, 2 fM to 50 pM miR-141 for 90 min, and 2 µM invaders (CI_{mis} + QI) for 20 min. All imaging was performed with 10% v/v formamide. All data are presented as mean ± s.d. of ≥ 3 independent experiments. iSiMREPS showed a linear dynamic range of approximately 3 fM - 5 pM which is approximately 3.2 orders of magnitude.

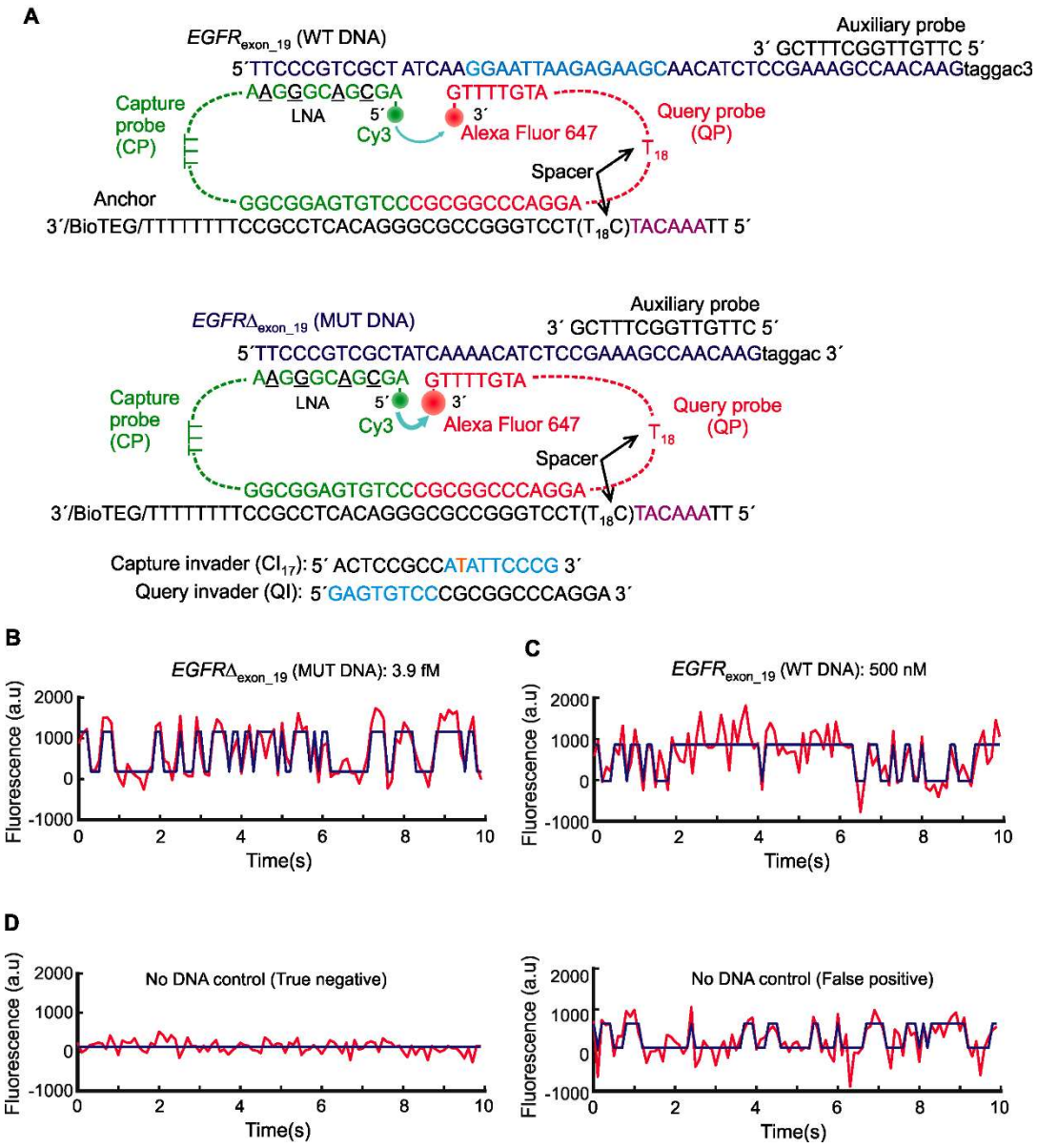

Fig. S14. Schematic of iSiMREPS sensor design for detecting *EGFR* exon 19 deletion mutant DNA (*EGFR*Δexon_19) and wild type DNA (*EGFR*exon_19) and representative single molecule kinetic traces. (**A**) Schematic of the iSiMREPS sensor for detection of *EGFR*Δexon_19and *EGFR*exon_19. The query probe was designed to be fully complementary to a short segment of the mutant DNA while lacking perfect complementarity with wild-type DNA. Representative single molecule kinetic traces for *EGFR*Δexon_19at 3.9 fM (**B**) and *EGFR*exon_19 at 500 nM (**C**). (**D**) Representative true negative and false positive single molecule kinetic traces for no DNA target (control).

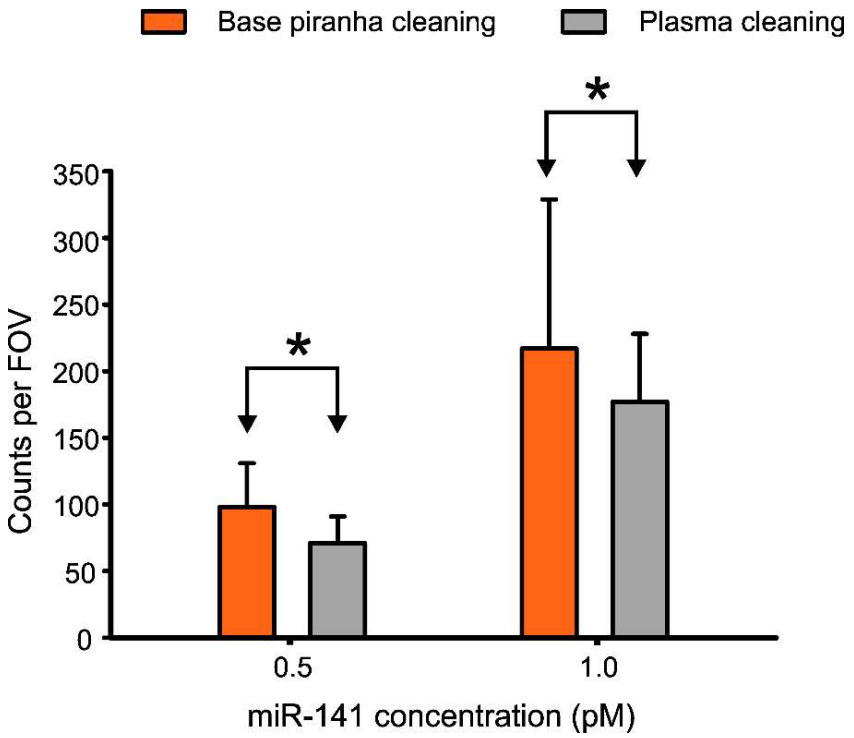

Fig. S15. Comparison of the performance of coverslip cleaning protocols for detecting miR-141. Base piranha cleaning protocol used a solution consisting of 14.3% v/v of 28-30 wt% NH_4OH, and 14.3% v/v of 30-35 wt% H_2O_2 that was heated to 70-80°C, whereas plasma cleaning protocol used application of plasma for 3 min to clean glass coverslip. The experiments were performed using a glass coverslip passivated with biotin-PEG: m-PEG at a ratio of 1:100, 10 nM sensor, 0.5 and 1.0 pM miR-141, and 2 μM invaders (CI_{mis} + QI). All imaging was performed with 10% v/v formamide. All data are presented as mean ± s.d. where n = 3 independent experiments. Single asterisk indicates the statistically insignificant differences at 95% confidence levels as assessed using a two-tailed, unpaired t test.

4 Supplementary References

Abelson, J., Blanco, M., Ditzler, M.A., Fuller, F., Aravamudhan, P., Wood, M., Villa, T., Ryan, D.E., Pleiss, J.A., Maeder, C., Guthrie, C., Walter, N.G., 2010. Nat. Struct. Mol. Biol. 17, 504-512.

Becker, N.B., Rosa, A., Everaers, R., 2010. E. Phys. J. E. 32, 53-69.

Blanco, M., Walter, N.G., 2010. Methods Enzymol. 472, 153-178.

Bronson, J.E., Fei, J., Hofman, J.M., Gonzalez, R.L., Jr., Wiggins, C.H., 2009. Biophys. J. 97, 3196-3205.

Caltech:, 2007.

Chatterjee, T., Li, Z., Khanna, K., Montoya, K., Tewari, M., Walter, N.G., Johnson-Buck, A., 2020. Trends Anal. Chem. 123, 115764.

Chen, H., Meisburger, S.P., Pabit, S.A., Sutton, J.L., Webb, W.W., Pollack, L., 2012. Proc. Natl. Acad. Sci. U. S. A. 109, 799.

Hayward, S.L., Lund, P.E., Kang, Q., Johnson-Buck, A., Tewari, M., Walter, N.G., 2018. J. Am. Chem. Soc. 140, 11755-11762.

Johnson-Buck, A., Li, J., Tewari, M., Walter, N.G., 2019. Methods 153, 3-12.

Marko, J.F., Siggia, E.D., 1995. Macromolecules 28, 8759-8770.

Saleh, O.A., McIntosh, D.B., Pincus, P., Ribeck, N., 2009. Phys. Rev. Lett. 102, 068301.

Seol, Y., Skinner, G.M., Visscher, K., 2004. Phys. Rev. Lett. 93, 118102.

Zadeh, J.N., Steenberg, C.D., Bois, J.S., Wolfe, B.R., Pierce, M.B., Khan, A.R., Dirks, R.M., Pierce, N.A., 2011. J. Comput. Chem. 32, 170-173.